Transportation Research Part D 91 (2021) 102688

Contents lists available at ScienceDirect

Transportation Research Part D

journal homepage: www.elsevier.com/locate/trd

On the design of environmentally sustainable aircraft for urban air mobility

Frederico Afonso [a], Ana Ferreira [a], Inês Ribeiro [a], Fernando Lau [a], Afzal Suleman [a,b,*]

[a] IDMEC, Instituto Superior Técnico, Universidade de Lisboa, Av. Rovisco Pais, No. 1, 1049-001 Lisboa, Portugal
[b] Department of Mechanical Engineering, University of Victoria, PO Box 1700, Stn. CSC, Victoria, British Columbia V8W 2Y2, Canada

ARTICLE INFO

Keywords:
Life cycle assessment
Hybrid-electric aircraft
Biofuels
Urban air mobility
Conceptual design

ABSTRACT

Urban Air Mobility (UAM), recently envisioned as faster and flexible mean of transportation in large urban centers, faces considerable challenges inherent in its operation in densely populated cities and related environmental issues such as pollutant and noise emissions. To address the environmental challenges, the proposed concepts are either hybrid-electric or all-electric vehicles enabled with propellers that rotate at lower speeds than conventional rotorcraft configurations, such as helicopters. However, the feasibility of UAM in the near future requires significant progress on the all-electric propulsion systems since current battery technology still falls short when compared with fossil fuel in terms of specific energy density. In this work, a methodology is proposed to evaluate the environmental footprint of Vertical Take-Off and Landing (VTOL) aircraft for the UAM market. This methodology is applied to existing concepts for exploratory studies on mission critical performance and environmental parameters. All-electric aircraft were found to be feasible for the UAM segment from the performance perspective. However, further improvements in battery technology and electricity generation from renewable sources are required. Sustainable aviation fuels, such as Alcohol-To-Jet (ATJ) obtained from wheat straw, present a substantially lower environmental impact than conventional fuels while providing the same performance. These biofuels also contribute less to global warming and climate changes than batteries which: (i) are recharged from electric grids still dependable on non-renewable sources; and (ii) have a low number of recharge–discharge cycles.

1. Introduction

In the recent past, substantial progress has been made on the development of Vertical Take-Off and Landing (VTOL) aircraft for the Urban Air Mobility (UAM) market. This is a new aviation segment that aims to transport passengers inside large urban centers in a faster and more flexible way than current transportation solutions such as bus, car, train or subway. Several authors claim that the maturity level in aviation technology already allows for the implementation of on-demand mobility using quiet, efficient and mainly automated air taxis (Thipphavong et al., 2018; Mueller et al., 2017; Rothfeld et al., 2020). However, the development of an air transportation platform for this segment requires overcoming several challenges in order to make it a safer, quieter and greener mode of transportation in densely populated urban areas. Challenges include: (i) establishing regulations for air traveling at low altitudes in

* Corresponding author at: Department of Mechanical Engineering, University of Victoria, PO Box 1700, Stn. CSC, Victoria, British Columbia V8W 2Y2, Canada.
E-mail address: suleman@uvic.ca (A. Suleman).

https://doi.org/10.1016/j.trd.2020.102688

Available online 20 January 2021
1361-9209/

urban areas, especially in what concerns air traffic management to ensure flight safety; (ii) proving the airworthiness of the envisioned aircraft concepts by performing flight tests; (iii) devising an efficient, reliable and light all-electric or hybrid-electric propulsive system (from the energy source up to the propeller/rotor) that can power these aircraft; (iv) integrating adequately the propulsive system into the air-frame such that both drag and noise are minimized; (v) designing an aircraft that can comply with noise regulations for operating in urban areas; (vi) minimizing vibrations caused by the propulsive system to improve passenger comfort; and (vii) building required infrastructures, such as helipads and charging stations.

From a social-economic point of view, there is also the public perception and acceptance, which needs to be favorable for this new way of transportation to be implemented (Eißfeldt, 2020). A recent survey on this subject has been presented by Al Haddad et al. (2020).

The environmental constraints for UAM adoption concern mainly noise and air quality issues. As noted in the Horizon 2020 – Work Programme 2018–2020 on Smart, Green and Integrated Transport, sustainability must consider the overall environmental footprint, noise and visual pollution (European Comission, 2020). According to Fu et al. (2019), the environmental impact related to UAM is still not adequately studied. This paper reports on critical issues related to the adoption of UAM in Munich, Germany, and assuming the aircraft to be energy efficient, emission free and quiet. Very few studies have addressed environmental sustainability aspects of UAM, while some have studied noise signature as this is one of the most critical constraints concerning community acceptance. An analysis on constraints for UAM implementation concluded that these are: (i) community acceptance of aircraft noise; (ii) take-off and landing area availability; (iii) and air traffic control scalability (Vascik et al., 2018). A study on sustainable air mobility states that UAM promises to foster sustainability and decarbonization, addressing only noise issues as the prominent limitation for air mobility in urban centers (Eißfeldt, 2020). This focus on noise over emissions and overall environmental foot print in UAM studies are based on the assumption that the aircraft are all-electric and therefore with no local pollutant emissions during flight operations. All-electric aircraft in fact do not have any direct air pollutants, but CO_2 emissions exist from the energy consumed in operations, which depends on the electric generation mix (Schäfer et al., 2019). Furthermore, hybrid solutions, although at a lower scale, consume fuel and contribute for local emissions. The fuel most commonly used in the aviation is the kerosene (Jet A-1) produced from crude oil. An alternate approach in the sustainable aviation area is the use of alternative and more sustainable jet fuel alternatives (Staples et al., 2018). This is one important step to invert the global dependence on fossil fuels and to comply with the International Air Transport Association (IATA) targets for 2050, for the global aviation industry to achieve carbon neutral growth by 2020 and reduce CO_2 emissions by 50% relative to 2005 levels by 2050. Sustainable fuels can decrease the CO_2 emissions, considering the life cycle, by up to 80% (International Air Transport Association, 2015).

Nowadays, the research focus is on biofuels production with similar properties or specifications to those of traditional Jet A-1 (Kerosene), with lower greenhouse gas (GHG) emissions on the production phase and in its utilization and with long term perspective. Currently, there are three synthetic fuel blends derived from different pathways certified by ASTM committee for commercial use: Fischer–Tropsch Synthetic Paraffinic Kerosene (FT-SPK), Hydro-processed Esters and Fatty Acids (HEFA) and ATJ (alcohol-to-jet). According with ASTM standards, FT-SPK, HEFA and ATJ are certified to be used in blending of up to 50% fossil jet fuel (Prussi et al., 2019).

The composition of the biofuels depends on the feedstock use for its production. Biofuels can be produced through biomass feedstock and considering different conversion processes. The Synthetic Fischer–Tropsch fuels are produced by a two-step process in which biomass is converted to a syngas through gasification, followed by syngas upgrading. This syngas is converted into bio-kerosene by the Fischer–Tropsch (FT) (STM International, 2020). Other HEFA fuels (Kousoulidou and Lonza, 2016; Neuling and Kaltschmitt, 2018, 2015) are produced by hydrogenation of biomass such as: soybean, canola, camelina, jatropha, following the isomerization to produce jet fuel, diesel and naphtha (Neuling and Kaltschmitt, 2018). ATJ fuel is produced by dehydration, oligomerization and hydroprocessing of ethanol or iso-butanol. The ethanol is produced by fermentation of biomass feedstock (de Jong et al., 2017). To study the biofuel production, a life cycle analysis is used to evaluate all production chain of biofuel from its production to its use considering the energy consumption, GHG emissions and pollutant emissions (Kousoulidou and Lonza, 2016; Neuling and Kaltschmitt, 2018; Lokesh et al., 2015; Han et al., 2013).

Despite the above mentioned technological, environmental and social-economic challenges, a multitude of aircraft concepts have been proposed over the past few years for the UAM segment, most of them all-electric, although hybrid versions with either fossil fuel or hydrogen have also being presented. The Vertical Flight Society has identified over 200 different concepts (Vertical Flight Society, 2020) categorized in: vectored thrust, lift + cruise, wingless and electric rotorcraft. Both range and passenger capacity vary considerably, with an upper limit of 700 nm and 16 passengers, and most of the concepts exhibit an average range of 190 nm and are only able to carry 1 to 4 passengers. A VTOL aircraft designed for this segment needs to combine the good hover performance of a helicopter with the good cruise performance of a fixed-wing; in other words, a low disk loading and a high lift-to-drag ratio are sought. These two goals are contradictory and thus an innovative propulsive system integration is required to achieve a good design compromise. In Zhou et al. (2020) an overview of possible VTOL configurations and technologies is provided for all aviation segments.

In this paper, a methodology to evaluate the feasibility of VTOL concepts for the UAM segment is presented and compared with existing methodologies (Section 2). Three different aircraft concepts with three possible propulsive systems are defined in Section 3 and a multidisciplinary design optimization study is carried out in Section 4. This study incorporates technological and sustainability constraints, and it addresses the design for a UAM aircraft from a multidisciplinary design perspective.

2. Methodology

A conceptual design methodology to evaluate the feasibility of VTOL concepts for the UAM segment is proposed. This methodology

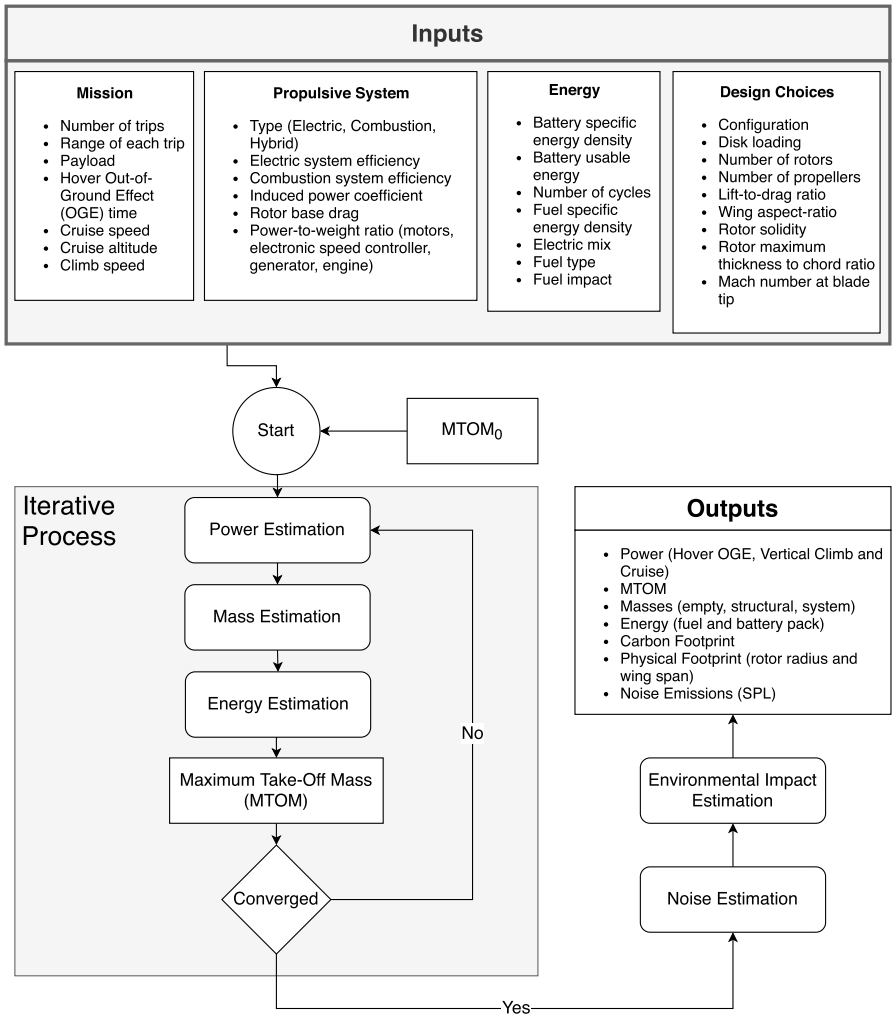

Fig. 1. Conceptual design methodology.

consists of an iterative process where power, mass, energy, environmental impact and noise emissions are estimated for the VTOL concept using analytical and semi-empirical equations and a set of inputs which are divided in four categories: mission, propulsive system, energy source and design choices. In this process, the Maximum Take-Off Mass (MTOM) is iterated until a converged solution is reached as in conventional aircraft design methodologies (Raymer, 1992; Cork, 2003). The output of this methodology is the initial sizing of the aircraft in terms of power, mass, energy, carbon and physical footprints and noise emissions. A flowchart of this methodology is depicted in Fig. 1.

2.1. Power estimation

To estimate the power requirements, the blade element moment theory (as described in Johnson, 2013) is used for the vertical flight, while an analytical expression is used for the horizontal flight. Two critical VTOL operations are considered, namely the hover power in Out-of-Ground-Effect (OGE) and the vertical climb. The hover in OGE (P_h), assuming that all rotors are equal and contribute the same, is calculated as follows

$$P_h = \sum_{j=1}^{\mathrm{NR}} T_j \left[k_i \sqrt{\frac{\mathrm{DL}}{2\rho}} + \frac{\rho V_{tip}^3}{\mathrm{DL}} \left(\frac{\sigma C_{d0}}{8} \right) \right], \tag{1}$$

where NR is the number of rotors considered, T_j is the thrust that each rotor j should produce (which is $(\mathrm{MTOM} \times g)/\mathrm{NR}$ due to the assumption that all rotors are equal and contribute equally to the overall power), k_i denotes the induced power factor, DL stands for disk loading, ρ denotes the air density, V_{tip} is the velocity at the tip of the rotor's blade, σ and C_{d0} are rotor's solidity and base drag, respectively. The power required for vertical climb, considering the same assumption as for hover, is given by

$$P_{cl} = \sum_{j=1}^{NR} T_j \left[V_y - \frac{k_i}{2} V_y + \frac{k_i}{2} \sqrt{V_y^2 + \frac{2DL}{\rho}} + \frac{\rho V_{tip}^3}{DL} \left(\frac{\sigma C_{d0}}{8} \right) \right], \tag{2}$$

where V_y is the vertical velocity. For cruise, the power required is estimated using the following analytical expression

$$P_{cr} = \frac{MTOM \times g \times V_{cr}}{L/D \times \eta_p}, \tag{3}$$

where g denotes the acceleration of gravity, V_{cr} is the cruise speed, L/D is the lift-to-drag ratio of the entire aircraft and η_p stands for propeller's efficiency.

2.2. Mass estimation

Statistical data is used to provide an initial estimation of the aircraft mass breakdown with the masses divided in five categories: payload, energy, propulsive system, structural and other weights. Payload is given as an input and energy is explained later, in sub-Section 2.3.

Structural mass (M_{str}), which includes the wing, rotors, empennage and fuselage, is estimated assuming a given structural factor (SF) similarly to conventional methodologies (Raymer, 1992; Cork, 2003) as follows

$$M_{str} = SF \times MTOM. \tag{4}$$

The propulsion mass (M_{prop}) depends on the propulsive system type, which can be all-electric, all-combustion or hybrid-electric. For an all-electric aircraft, only electric motors are considered; while for an all-combustion aircraft an internal combustion engine is accounted for and possibly, depending on the configuration, a generator and electric motors can be included. In a hybrid aircraft, a combustion engine, a generator and electric motors are all taken into account. To estimate the mass of the electric motor (M_{em}), including the electronic speed controller and its integration, three factors are introduced: the power-to-weight-ratio of the electric motor (PWe); the power-to-weight-ratio of the electronic speed controller (PWesc); and the integration factor (MI). These factors are integrated as follows

$$M_{em} = \left[\left(\frac{P_{cl}}{PWe} \right) + \left(\frac{P_{cl}}{PWesc} \right) \right] MI. \tag{5}$$

The combustion engine is also estimated based on a given power-to-weight ratio (PWc) from existing combustion engines

$$M_{ce} = \frac{P}{PWc}. \tag{6}$$

The same approach is followed for the generator

$$M_g = \frac{P}{PWg}, \tag{7}$$

where PWg is the power-to-weight-ratio of the generator.

Aircraft systems such as avionics, flight control, instrumentation, environmental control and furnishing, are accounted for as a fraction (OW) of the empty mass (M_{empty}), as in Ng (2019). The empty mass is then given by

$$M_{empty} = \frac{M_{str} + M_{prop}}{1 - OW}, \tag{8}$$

where $M_{prop} = M_{em} + M_{ce} + M_g$.

2.3. Energy estimation

The required amount of energy stored in the aircraft is estimated based on the established mission and propulsive system strategy (all-electric, all-combustion and hybrid-electric). To simplify the mission definition, only hover and cruise segment are accounted for in the energy estimation. Endurance time (t_E) (calculated based on cruise speed and range) with a reserve time (t_R) of 20 min (based on certification for rotorcraft (Johnson et al., 2018)) is considered for cruise operation, while a hover time (t_H) corresponding to 60 s for each take-off and landing operation is assumed for the vertical flight.

For an all-electric aircraft, the energy (E_{bat}) and the mass of the required battery pack (M_{bat}) can be estimated as follows

$$E_{bat} = \frac{\left[\frac{P_h}{\eta_{ES}} t_H + \frac{P_c}{\eta_{ES}} (t_E + t_R) \right]}{(1 - E_{bat,r})}, \tag{9}$$

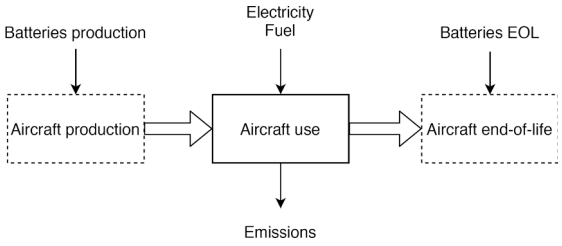

Fig. 2. Scope of the life cycle assessment.

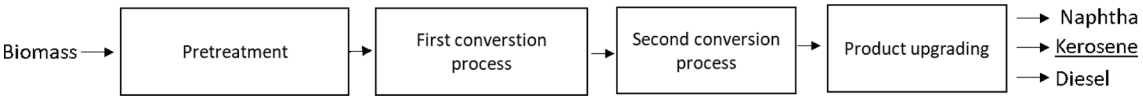

Fig. 3. A schematic overview of the whole process of the biofuel production.

$$M_{bat} = \frac{E_{bat}}{E^*_{bat}}, \tag{10}$$

where η_{ES} is the efficiency of the electric system (i.e. the power train efficiency) for each segment (hover and cruise) which might change with the aircraft configuration, E^*_{bat} denotes the specific energy density of the battery pack and the $E_{bat,r}$ parameter stands for the non-usable battery percentage to improve its life cycle. Analogously, for an all-combustion aircraft the fuel energy (E_{fuel}) and mass (M_{fuel}) are given by the following expressions:

$$E_{fuel} = \left[\frac{P_h}{\eta_{CS}} t_H + \frac{P_c}{\eta_{CS}} (t_E + t_R)\right] 1.05, \tag{11}$$

$$M_{fuel} = \frac{E_{fuel}}{E^*_{fuel}}, \tag{12}$$

where η_{CS} is the efficiency of the combustion system (which also depends on the configuration and mission segment). Fuel trapped is assumed to be 5% of the overall fuel mass (this is a conservative value and is normally considered for commercial aircraft, 1% (Cork, 2003)) and E^*_{fuel} denotes the specific energy density of the fuel considered.

In a hybrid-electric aircraft, take-off, landing and vertical climb operations are set to be all-electric (i.e. resorting only to batteries), since these aircraft are to be operated in urban areas; while in cruise a hybridization factor (ϕ) is used to determine the fuel energy and the remaining energy of the battery pack (Eq. 13), which can be converted in mass using Eqs. 12 and 10, respectively:

$$\begin{cases} E_{bat} = \dfrac{\left[\dfrac{P_h}{\eta_{ES}} t_H + \phi \dfrac{P_c}{\eta_{ES}} (t_E + t_R)\right]}{(1 - E_{bat,r})} \\ E_{fuel} = (1 - \phi) \dfrac{P_c}{\eta_{CS}} (t_E + t_R) 1.05 \end{cases} \tag{13}$$

2.4. Environmental impact estimation

The environmental impact estimation is expressed in the unit of kilogram of carbon dioxide equivalent per functional unit (kg CO_2-eq), a metric for global warming potential (GWP) of the Life Cycle Assessment (LCA) methodology. GWP is the most widely used metric, addressed in nearly every LCA, and is the focus of carbon footprinting (Jungbluth and Meili, 2019). Different greenhouse gases such as methane (CH_4) or dinitrogen monoxide (N_2O) are expressed as kg CO_2-eq through characterization factors assessing their relative impact to climate change (CC). The GWP is computed through the ReCiPe Midpoint/Endpoint (H) V1.11/ Europe Recipe H method with the support of LCA software (SimaPro) and the Eco Invent database.

This analysis follows a consequential LCA approach, aiming to identify the differences on the impact between UAM alternatives. Since all alternatives are aircraft based, only the batteries are included in the aircraft production and end-of-life phases (see Fig. 2). Regarding the use phase, the resources used in the aircraft operations are electricity in the all-electric alternatives and electricity and fuel in the hybrid alternatives. The direct emissions will be considered in the case of hybrid aircraft. The emissions data used for battery production (80.8 kgCO_2-eq/kW.h) and EOL (1.09 kgCO_2-eq/kW.h) is based on a previous study (Ribeiro et al., 2020).

Relatively to the biofuels production, the data used is based on literature data (Neuling and Kaltschmitt, 2018; Lokesh et al., 2015). The life cycle analysis considers the whole biofuel production chain and includes the cultivation of the feedstock, transportation, pre-

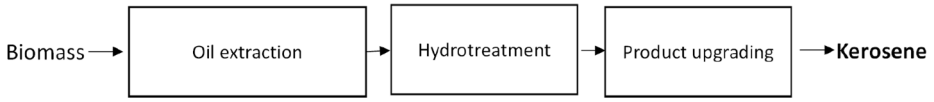

(a) Fischer-Tropsch Synthetic Paraffinic Kerosene

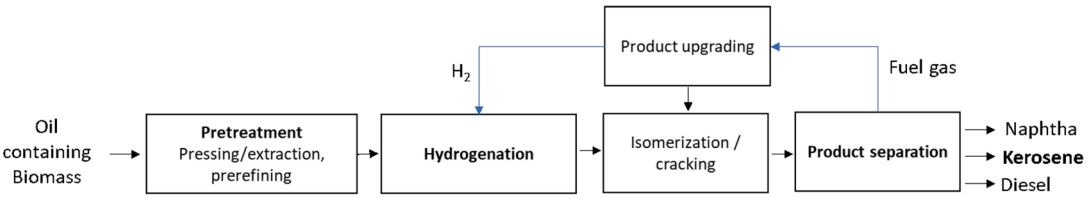

(b) Hydro-processed Esters and Fatty Acids (adapted from (Neuling and Kaltschmitt, 2018))

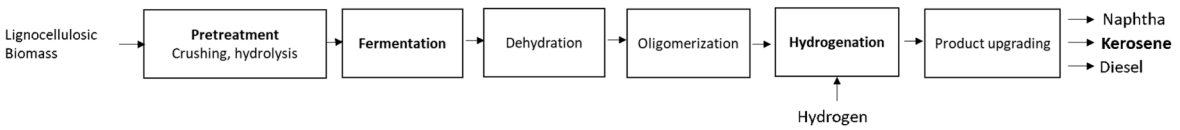

(c) Alcohol-To-Jet (adapted from (Neuling and Kaltschmitt, 2018))

Fig. 4. A schematic overview of the supply chain of the FT-SPK (a), HEFA (b) and ATJ (c).

Table 1
CO_2 equivalent in the production of different energy sources.

Energy Source	Emissions	Unit	Comment	Reference
Li-S battery system	80.8	($kgCO_2$-eq/kW.h)		Ribeiro et al. (2020)
Electricity	294	(gCO_2-eq/kW.h)	European Union (EU-28)	IEA (2019)
Jet Fuel A	87.5	(gCO_2-eq/$MJ_{Kerosene}$)		Neuling and Kaltschmitt (2018)
FT-SPK	30.7	(gCO_2-eq/$MJ_{Kerosene}$)	from camelina	Lokesh et al. (2015)
	37.9	(gCO_2-eq/$MJ_{Kerosene}$)	from jatropha	Lokesh et al. (2015)
	39.7	(gCO_2-eq/$MJ_{Kerosene}$)	from microalgae	Lokesh et al. (2015)
HEFA	52.0	(gCO_2-eq/$MJ_{Kerosene}$)	from palm oil	Neuling and Kaltschmitt (2018)
	73.5	(gCO_2-eq/$MJ_{Kerosene}$)	from jatropha	Neuling and Kaltschmitt (2018)
ATJ-SPK	30.4	(gCO_2-eq/$MJ_{Kerosene}$)	from wheat straw	Neuling and Kaltschmitt (2018)
	70.3	(gCO_2-eq/$MJ_{Kerosene}$)	from wheat grain	Neuling and Kaltschmitt (2018)

treatment and conversion process. Fig. 3 shows a schematic overview of the whole process of the biofuel production. The functional unit is 1 MJ of produced kerosene. Different pathways of production considering different biomass sources are compared. The camelina, jatropha and microalgae biomass are considered for FT-SPK production, the jatropha and palm oil for HEFA production and wheat straw and wheat grain for ATJ production. These case studies are chosen in terms of biomass availability. The production pathways of the specific biofuels considered in this study are present in Fig. 4.

The usage of biofuel is also considered. Since the data of the emission of biofuel usage will not be assessed, a conversion factor of 8.887 grams of CO_2-eq per gallon of fuel consumed will be assumed. This value is estimated by the Environmental Protection Agency for an average gasoline car (EPA, 2020). However, the fossil fuel replacement by biofuel can reduce 80% of CO_2-eq emissions.

A value of 294 gCO_2-eq/kW.h for the European Union (EU-28) electric grid (IEA, 2019) is considered for process of recharging the battery system.

Regarding the production phase, the following GWP presented in Table 1 is used for each resource and emission.

Both use ($Emissions_{Use}$) and production ($Emissions_{Prod}$) emissions of the energy sources are estimated in the developed computational model. For the use phase both the battery recharge and fuel consumed are accounted for, as follows:

$$\text{Emissions}_{Use} = \left(E_{fuel}\left(\text{Emissions}_c^* + \text{Emissions}_f^*\right) + E_{bat} \times \text{Emissions}_e^*\right) N_{cycles}, \tag{14}$$

where Emissions_c^*, Emissions_f^* and Emissions_e^* denote the emissions generated per functional unit by the fuel consumed during the use phase (in gCO_2-eq/$MJ_{Kerosene}$), by the production of this fuel consumed (in gCO_2-eq/$MJ_{Kerosene}$) and by the electric grid (in gCO_2-eq/kW.

h) used to recharge the batteries, respectively. To note that the maximum number of battery recharge cycles (N_{cycles}) is assumed in this estimation to simulate the entire battery life. The emissions related to the production phase are associated only to the production of the batteries (Emissions_b^* in gCO_2-eq/kW.h) as given by

$$\text{Emissions}_{Prod} = E_{bat} \times \text{Emissions}_b^*. \tag{15}$$

These two contributions are latter summed with the batteries EOL contribution to estimate the overall emissions as follows,

$$\text{Emissions}_{Total} = \text{Emissions}_{Use} + \text{Emissions}_{Prod} + E_{bat} \times \text{Emissions}_{bat,EOL}^*, \tag{16}$$

where $\text{Emissions}_{bat,EOL}^*$ represents the emissions generated by the batteries per functional unit (gCO_2-eq/kW.h) in the EOL phase.

2.5. Size estimation

After the iterative process has converged, the rotor's radius r and wing area S are estimated. The former is a simple calculation based on the disk loading and the number of rotors (NR),

$$r = \sqrt{\frac{\text{MTOM} \times g}{\pi \times \text{NR} \times \text{DL}}}; \tag{17}$$

while the latter can be estimated based on the selected wing loading (W/S) constraint. Two wing loading constraints are modeled:

1. Stall speed

$$\frac{W}{S} = \frac{1}{2}\rho V_{stall}^2 C_{L,max}; \tag{18}$$

2. Range

$$\frac{W}{S} = \frac{1}{2}\rho V_{cr}^2 \frac{\pi \text{AR} e}{2L/D}. \tag{19}$$

In the above equation V_{stall} is the stall speed (65 kts (33.4 m/s) is considered based on EASA CS-23), $C_{L,max}$ stands for the maximum lift coefficient (a value of 1.2 is employed, which is a lower limit for civil light aircraft (Cork, 2003)), e denotes the Oswald efficiency factor (assumed to be equal to 0.8) and AR is the wing aspect-ratio.

2.6. Aeroacoustic model

There are several sources contributing to noise emission in a VTOL aircraft, including thermal engine, rotor, electric motor, gear-box and other rotating internal components. Here, following the work reported by Brown and Harris (2018), only the noise generated by the rotors is considered. The noise emitted by the gear-box, internal rotating components and electric motors is neglected in this study. Rotor noise can be classified as rotational, impulsive and vortex by increasing frequency value (Johnson, 2013). Rotational noise normally leads to the highest Sound Pressure Level (SPL) in the sound spectrum, but in a conventional helicopter these are present in the low frequency range, sometimes even below the human hearing threshold (Johnson, 2013). However, this noise source can occur in UAM rotorcraft at higher frequencies than what normally happens in a conventional helicopter since the size of the rotors is considerably smaller. Impulsive noise, also known as blade slap, is another source, which occurs at some flight conditions when the blade enters stall, when shock waves are formed on its surface, or when blade-vortex interactions occur. These issues can be avoided or mitigated according to Brown and Harris (2018), respectively, by properly designing the airfoil blade, by lowering the possible Mach number at the blade tip (within 0.3 and 0.55), and by applying adequate flight procedures. For these reasons, impulsive noise is not accounted for in this work. Vortex noise (also known as broadband noise) occurs at higher frequencies and results from the interaction between flow turbulence and loads fluctuations on the blades (Johnson, 2013). Thus, adequate design considerations must be addressed when designing the blades and their operation in UAM aircraft. It is also worth mentioning that acoustic noise emissions from similar aircraft configurations, although at a smaller scale, have been subject of study from several groups given the highest impact that it is expected of them to have in urban areas when compared to road vehicles (Torija et al., 2020).

2.6.1. Rotational noise

To predict the rotational noise, semi-empirical expressions as described in Brown and Harris (2018) are used. This noise source can be split into loading and thickness noise which are modeled in Brown and Harris (2018) using the formulation by Gutin (1948) and Deming (Deming, 1940), respectively. First the root mean square of the loading and thickness noise pressures (p_{m_L} and p_{m_T}, respectively) are estimated:

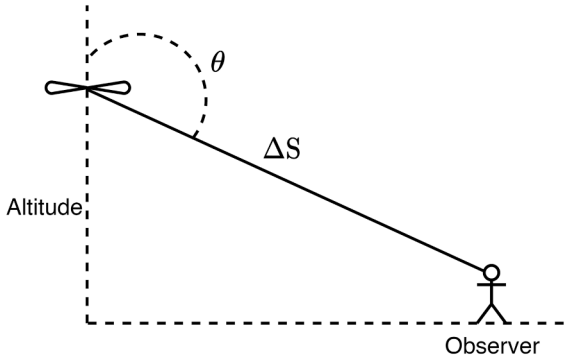

Fig. 5. Definition of the θ angle in reference to the rotor and observer.

$$p_{m_L} = \frac{m\mathrm{NB}\Omega}{2\sqrt{2}\pi a \Delta S}\left[T cos\theta - Q\frac{a}{\Omega r_e^2}\right] J_{m\mathrm{NB}}\left(\frac{m\mathrm{NB}\Omega}{a} r_e sin\theta\right), \tag{20}$$

$$p_{m_T} = \frac{-\rho(m\mathrm{NB}\Omega)^2 \mathrm{NB}}{3\sqrt{2}\pi\Delta S} c t_{max} r_e J_{m\mathrm{NB}}\left(\frac{m\mathrm{NB}\Omega}{a} r_e sin\theta\right), \tag{21}$$

where m corresponds to the harmonic number (in this study only the first harmonic is considered), NB denotes the number of blades, Ω is the angular speed of the rotor, a stands for speed of sound, ΔS denotes distance between the observer and rotor as illustrated in Fig. 5, T and Q are respectively rotor thrust and torque, θ is defined as depicted in Fig. 5, r_e corresponds to the effective radius (here set as 80% of the rotor's radius as it is used in Brown and Harris (2018)), $J_{m\mathrm{NB}}$ is the first kind Bessel function of mNB order, ρ denotes air density, c and t_{max} are the chord and maximum thickness of the blade, respectively.

After estimating the two contributions, the SPL for a single rotor can be obtained as follows:

$$\mathrm{SPL} = 10 log_{10}\left[\frac{p_{m_L}^2 + p_{m_T}^2}{p_{ref}^2}\right], \tag{22}$$

where p_{ref} corresponds to the reference pressure set to 20μPa. This equation can be rewritten to incorporate the noise from all rotors:

$$\mathrm{SPL} = 10 log_{10}\left[\mathrm{NR}\left(\frac{p_{m_L}^2 + p_{m_T}^2}{p_{ref}^2}\right)\right]. \tag{23}$$

Such expression requires assuming that the noise from each rotor is noncoherent, which is seen as a typically good first estimation according to Brown and Harris (2018).

2.6.2. Vortex noise

Vortex noise is predicted also based on a semi-empirical model, in this case, the Schlegel et al. (1966) model built and validated for helicopters, and described in Marte and Kurtz (1970) and Brown and Harris (2018). Due to the unconventional nature of some VTOL concepts when compared with conventional helicopters, involving complex unsteady aerodynamics, this model is not accurate. Nevertheless, at a conceptual design level, it can still provide useful vortex noise trends (Brown and Harris, 2018). In this model, the SPL for a hover condition is calculated as follows:

$$\mathrm{SPL} = 20 log_{10}\left[k_2 \frac{V_{tip}}{\rho \Delta S}\sqrt{\frac{\mathrm{NR}T}{\sigma}\mathrm{DL}}\right], \tag{24}$$

where k_2 is a parameter set constant to 1.206×10^{-2} s^3/ft^3 (4.259×10^{-1} s^3/m^3, value calibrated for helicopters). However, this equation does not provide information for the frequency spectrum of interest identified by Schlegel et al. (1966) in their experimental work. In this frequency spectrum the peak frequency f_{peak} is given by:

$$f_{peak} = \frac{St 0.7 V_{tip}}{t_{max} cos\left(\frac{\overline{C_l}}{2\pi}\right) + c sin\left(\frac{\overline{C_l}}{2\pi}\right)}, \tag{25}$$

where St is the Strouhal number (a constant value of 0.28 (Marte and Kurtz, 1970), typical for helicopter, is considered) and $\overline{C_l}$ denotes the mean lift coefficient of the rotor, which is determined from the rotor's thrust coefficient (C_T) as follows:

Table 2
Comparison of the results for an all-electric aircraft with different numerical tools (NDARC and SUAVE data are from Vegh et al. (2019)).

Parameter	Estimated	NDARC	SUAVE	Δ NDARC	Δ SUAVE
MTOM (lb)	2086	2233	2086	7%	0%
Empty Mass (lb)	1687	1834	1686	8%	0%
Structural Mass (lb)	585	701	505	17%	15%
Propulsive System Mass (lb)	294	494	485	41%	39%
Systems Mass (lb)	248	249	245	1%	1%
Payload (lb)	400	400	400	0%	0%
Battery Pack Mass (lb)	561	372	444	51%	26%
Hover Power (hp)	412	410	375	0%	10%
Vertical Climb Power (hp)	427	445	400	4%	7%
Cruise Power (hp)	78	75	95	4%	18%
Rotor Radius (ft)	1.7	2.0	2.0	13%	13%
Wing area (ft^2)	122	114	114	7%	7%

$$\overline{C_l} = \frac{3C_T}{\sigma} = \frac{6T}{\rho V_{tip}^2 \mathrm{NB}cr}. \tag{26}$$

Octave bands with respect to the peak frequency were experimentally obtained by Schlegel et al. (1966) to tune the SPL value emitted by the rotor vortex in this domain, given in dB as described in Brown and Harris (2018) and Marte and Kurtz (1970) to sum all contributions and estimate the total vortex SPL.

2.7. Numerical comparison

Due to the lack of information and the embryonic nature of VTOL aircraft development for UAM segment, the methodology here presented is compared to numerical results from different design tools used for the same purpose. This data is presented by Vegh et al. (2019), where the authors compare the capabilities of two open-source conceptual aircraft design frameworks, NDARC (Johnson, 2010; Johnson et al., 2018) and SUAVE (Lukaczyk et al., 2015; Vegh et al., 2019) in designing electric VTOL aircraft applied to the Kitty Hawk Cora aircraft (now Wisk Cora aircraft(Wisk Aero LLC, 2020)), a lift + cruise configuration with 12 vertical rotors and 1 forward pusher propeller. The available information from the paper complemented with data from Bacchini and Cestino (2019) (where the same aircraft is also studied) are used as inputs in the current study. Average values between NDARC and SUAVE are considered for the lift-to-drag ratio (10.6), figure of merit (0.637) and propeller efficiency (0.823) which are inputs in the current method, except the figure of merit which is used to tune the rotor base drag.

Both NDARC and SUAVE numerical methods, described respectively in Johnson (2010), Johnson et al. (2018) and Lukaczyk et al. (2015), Vegh et al. (2019), have different approaches than the methodology developed here, namely in what concerns the fidelity and level of detail employed. For instance, in the mentioned numerical tools, the aerodynamic drag is built-up based on the aircraft geometry, while in the tool developed here the drag is considered via inputs at a higher level such as lift-to-drag ratio and rotor base drag. Also, the electric propulsive system (battery, electronic speed controller and motor) is modeled using empirical expression in both NDARC and SUAVE, while in the current method a power-to-weight ratio and an integration factor are used instead. Regarding structural mass estimation, NDARC recurs to empirical expressions generated from a rotorcraft database (for the wing, rotors, fuselage and empennage) and SUAVE uses a structural model (also for the wing, rotors, fuselage and empennage), while only a structural factor is employed here.

The results for the all-electric VTOL aircraft are presented in Table 2, and a comparison to the results from NDARC and SUAVE reported in Vegh et al. (2019) are also included. Despite the difference in the methodologies, the results are generally in good agreement, especially the MTOM and the power estimations. Both MTOM and empty mass compare well, although both the structural mass and propulsive system mass are underestimated and the battery pack is overestimated. With respect to the mass of the structure and propulsive system, the observed differences were expected given how both variables are modeled, as previously mentioned. Regarding the battery pack mass difference, while the entire mission is modelled in SUAVE, a simplified approach is used here, where the hover time is used to simulate the energy consumed in the vertical operations (take-off, vertical climb and landing). Due to this simplification, a conservative value is obtained providing a higher mass for the battery pack. The values estimated for power are similar to those predicted using NDARC and SUAVE. There is a 13% difference in the rotor radius due to the way how the implemented model works. In the current model, the disk loading (880 N/m^2) is provided as an input instead of the rotor radius (as in NDARC and SUAVE). To obtain the wing area, the stall speed constraint was used with typical values for stall speed and maximum lift coefficient (65 kts (33.4 m/s) and 1.2, respectively, as mentioned before), yielding a small error of 7%. Given the relatively good agreement with the other two conceptual design tools, the current methodology is deemed acceptable to conceptually design VTOL concepts for the UAM segment.

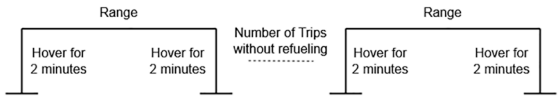

Fig. 6. Mission profile.

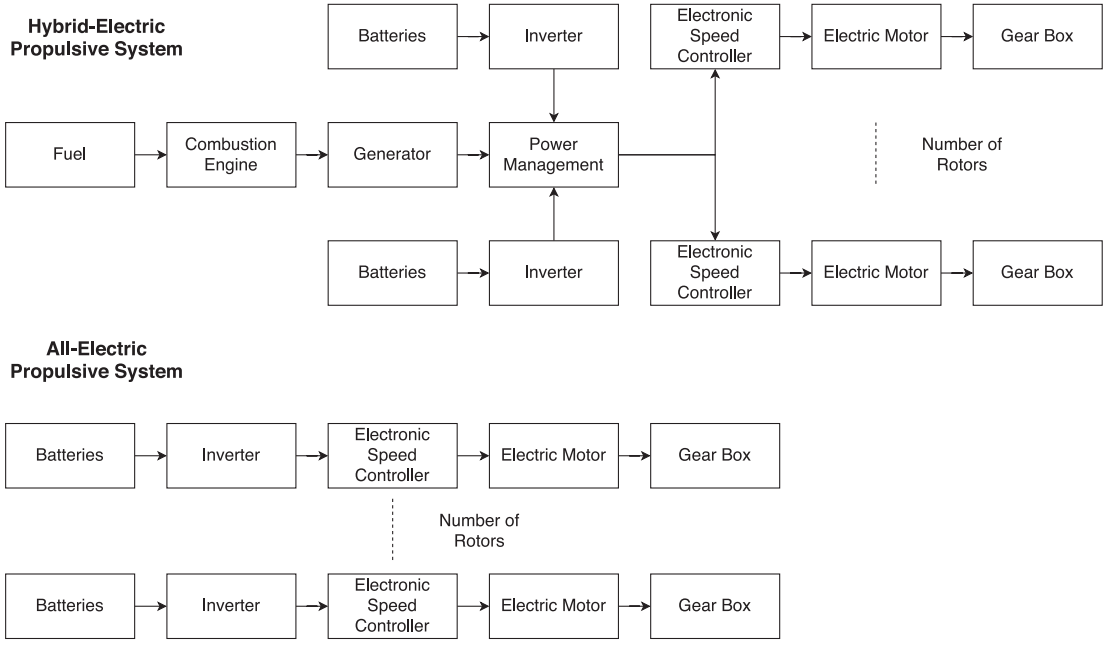

Fig. 7. Propulsive system.

3. Aircraft concepts

For this study, three different aircraft concepts are selected, which aim to combine a low disk loading with a high lift-to-drag ratio to achieve good performance for both vertical and horizontal flights. These are:

1. Lift + Cruise – configuration with 2 separate propulsive systems, one for vertical operations and another for horizontal flight;
2. Tilt-rotor – aircraft where the propulsive system adjusts to each flight condition;
3. Tilt-wing – concept with a adaptable wing depending on the flight condition.

In order to improve performance in both vertical and horizontal flight, these concepts adapt to these conditions either by changing the propulsive system operation or by moving its wing or propulsive system. The former might be more efficient and simpler from the propulsion point of view since each propulsive system is optimized for its operation at a possible cost of higher aerodynamic drag; while the latter configurations might be more aerodynamically efficient, although they are more complex, possibly heavier (due to the tilt mechanism) and the propulsive system might not be operating optimally at both flight conditions. There are lift + cruise and tilt-wing concepts being flight tested at their full size for the UAM segment, which are the cases of the Aurora/Boeing Passenger Air Vehicle (Aurora Flight Sciences, 2020) and the Airbus Vahana (Airbus, 2020), respectively. Regarding the tilt-rotor configuration, there is already a military aircraft certified for flight for more than a decade, the Bell Boeing V-22 Osprey (Boeing Company, 2020).

These selected aircraft concepts are designed for a simplified standard mission repeated over a given number of trips without refueling or battery recharge or replacement (see Fig. 6). The standard mission is characterized by: 4 min of hover time, 2 for take-off and 2 for landing, at OGE and sea level (considering ISA [1] + 20°C) conditions to account for vertical operations; and a cruise segment at 5000 ft (1524 m) for a given range. A similar mission profile is considered in Johnson et al. (2018). The number of trips is set to 4 as in Johnson et al. (2018) for a 6 passenger side-by-side helicopter. A vertical climb rate of 500 ft/min (2.54 m/s) is chosen to size the power at vertical climb, also considering ISA + 20°C conditions at sea level. Cruise speed (50–150 kts (25.7–77.1 m/s)), range (20–60 nm (37–111 km)) and payload (300–1200 lbs (136–544 kg)) are set as design variables depending on the propulsive system and configuration.

[1] International Standard Atmosphere

Table 3
Comparison of the results for an all-electric aircraft with different numerical tools.

Component	Efficiency	Reference
Combustion Engine	50%	Hepperle (2012) and Kuhn et al. (2012)
Generator	99%	Kuhn et al. (2012)
Power Management	95%	Kuhn et al. (2012)
Inverter	99.5%	Pornet et al. (2015)
Electronic Speed Controller	98%	Hepperle (2012)
Electric Motor	95%	Hepperle (2012)
Gear-Box	98%	Hepperle (2012)

Table 4
Specific energy density of the selected biofuels.

Fuel	Specific Energy Density (MJ/kg)	Reference
FT-SPK	44.2	Chuck (2016)
HEFA	43.70	Gawron (2018)
ATJ-SPK	43.20	GEVO (2020-06-2)
Kerosene	43.28	Gutiérrez-Antonio et al. (2017)

Table 5
Design choices for 3 concepts.

Configuration	L/D (-)	DL (lb/ft^2)	NR (–)	NP (–)	AR (–)	η_p (%)	SF (–)	OW (–)	MI (–)
Lift + Cruise	8–12	10–20	8	1	6–10	80	0.28	0.22	1.55
Tilt-rotor	12–16	10–20	12	0	6–10	76	0.30	0.22	1.55
Tilt-wing	10–14	10–20	8	0	6–10	76	0.30	0.22	1.55

As mentioned before, three different types of propulsive systems are analyzed: all-electric; all-combustion; and hybrid-electric. The power-trains of these systems are illustrated in Fig. 7 and the efficiency of their constituting components are summarized in Table 3. In what concerns the rotor design, initially a 550 ft/s (167.64 m/s) limit for speed at the blade tip to reduce noise (Johnson et al., 2018) is set and the following assumptions based on (Brown and Harris, 2018) are considered: $k_i = 1.2; C_{d0} = 0.01$; and $\sigma = 0.1$. However, when a noise constraint is added to the optimization problem three new design variables are added: the Mach number at the blades' tip M_{tip} (between 0.3 and 0.5); the rotors' solidity σ (allow to vary within 0.1 and 0.2); and the maximum thickness to chord ratio of the blades t/c_{max} (allowing it to be up to 25% thicker than 0.12 value used in Brown and Harris (2018) [2]). The power-to-weight ratio of the motor, generator, electronic speed controller and combustion engine are set to 5, 5, 20 and 3.29 kW/kg, respectively, again based on the literature (Patterson et al., 2012; Finger et al., 2019; Johnson et al., 2018).

Despite the use of Li-ion batteries being more widespread, namely in the automotive sector (Bini et al., 2015), Li-S batteries are chosen for this study. The main reason for this choice is related to the higher specific energy density that the latter presents in comparison to the former. Current state of the art Li-ion batteries have a specific energy density of around 250 W.h/kg (Zubi et al., 2018), while the Li-S technology varies between 300 and 500 W.h/kg (Benveniste et al., 2018). Here the upper value is considered (i.e. $E^*_{bat} = 500$ W.h/kg), which is considerably lower than the values of fossil fuels (over 10,000 W.h/kg). To improve the battery life, only 70% of its energy is assumed as usable (i.e. $E_{bat,r} = 0.3$). Accordingly to Wolff et al. (2019) up to 500 recharge–discharge cycles are possible with these batteries in the mentioned conditions.

Besides batteries also other greener solutions are considered in this work such as sustainable aviation fuels, namely biofuels. These consist in a mixture between fossil fuels and renewable hydrocarbons which can vary depending on the origin and production (Gutiérrez-Antonio et al., 2017). For this study, 3 biofuels already at high Technical Readiness Levels (TRLs) and approved by the American Society for Testing and Materials (ASTM) (Prussi et al., 2019) are selected: Fischer–Tropsch Synthetic Paraffinic Kerosene (FT-SPK); Hydro-processed Esters and Fatty Acids (HEFA); and Alcohol-to-Jet- Synthetic Paraffinic Kerosene (ATJ-SPK). The specific energy densities of these biofuels alongside Kerosene are summarized in Table 4.

The design choices of lift-to-drag ratio and disk loading for these concepts are based on the range values indicated by McDonald and German at the Uber Elevate Summit in 2017 (McDonald and German, 2017). The number of rotors is set to be the same as in Brown and Harris (2018), which is based on similar VTOL concepts (Aurora/Boeing Passenger Air Vehicle (Aurora Flight Sciences, 2020), Joby S2 (Vertical Flight Society, 2020-05-2) and Airbus Vahana (Airbus, 2020)), while the number of propellers NP, the range of wing aspect-ratio and the propeller's efficiency are assumed and the ratios SF, OW and MI are tuned for the numerical comparison problem (Section 2). All these design choices are listed in Table 5. A 5% decrease in the propeller efficiency and an increase of 5% in the structural factor are assumed for the tilt-rotor and tilt-wing configurations, which are inherent to the propulsive system not being optimally designed

[2] To note that in the method presented here, the t/c_{max} parameter only has impact on the thickness component of the rotational noise.

Table 6
Upper and lower boundaries set for the selected design variables.

Configuration	L/D (–)	DL (lb/ft^2)	AR (–)	V_{cr} (kts)	Range (nm)	Payload (lb)	M_{tip} (–)	σ (–)	t/c_{max} (–)
Lift + Cruise	8–12	10–20	6–10	50–150	20–60	300–1200	0.3–0.5	0.1–0.2	0.12–0.15
Tilt-rotor	12–16	10–20	6–10	50–150	20–60	300–1200	0.3–0.5	0.1–0.2	0.12–0.15
Tilt-wing	10–14	10–20	6–10	50–150	20–60	300–1200	0.3–0.5	0.1–0.2	0.12–0.15

Table 7
Results for the Payload-Range multi-objective optimization. L + C, TR and TW stand for the analyzed configurations: Lift + Cruise, Tilt-rotor and Tilt-wing, respectively. R and P denote the range and payload objectives.

Config.	Obj.	Range (nm)	Payload (lb)	PAX	MTOM (lb)	Speed (kt)	L/D (–)	DL (lb/ft2)	Power (hp)	Energy (kW.h)	b (ft)	20 nm Trips (–)	Time p/ Trip (min)
L + C	R	206	300	1	5506	79	12.00	10.58	666	609	50	12	15
	P	116	1200	5	5621	80	12.00	10.09	668	421	50	8	15
TR	R	240	331	1	5492	100	15.99	10.00	651	571	50	13	12
	P	133	1200	5	5657	92	16.00	10.00	670	393	50	9	13
TW	R	213	300	1	5570	86	14.00	10.42	670	585	50	12	14
	P	112	1200	5	5655	93	14.00	10.00	670	393	50	8	13

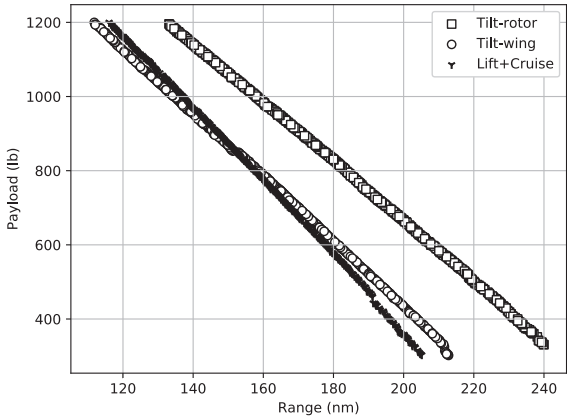

Fig. 8. Pareto Front for the Payload-Range multi-objective optimization.

for cruise and due to tilting mechanism, respectively.

4. Results

With the parameters and design choices established in Section 3, it is now possible to formulate a multi-objective optimization problem (Eq. 27) with three goals: total range [3] maximization; payload capacity maximization; and emissions minimization:

$$\begin{aligned} &\text{minimize} && f(-\text{Total Range}, -\text{Payload}, \text{Emissions}) \\ &\text{with respect to} && x = (L/D, \text{DL}, \text{AR}, V_{cr}, \text{Range}, \text{Payload}, M_{tip}, \sigma, t/c_{max}) \\ &\text{subject to} && max(P_h, P_{cl}, P_{cr}) \leqslant 670\text{hp} \\ & && b \leqslant 50\text{ft} \\ & && max(SPL) \leqslant 65\text{ dB} \end{aligned} \tag{27}$$

The selected design variables (x) are the lift-to-drag ratio, disk loading, aspect-ratio, cruise speed, range of each trip, payload, Mach number at the blades' tip, rotor's solidity and maximum thickness to chord ratio of the blades (these last three are only employed when a noise constraint is included in the optimization). Their upper and lower boundaries are summarized in Table 6. The constraints are the maximum power and wingspan which should not exceed 670 hp (500 kW) and 50 ft (15.24 m), respectively. Additionally, a noise limit of 65 dB for the aircraft hovering at an altitude of 500 ft (152.4 m) is imposed as a constraint to mitigate the noise impact on the urban environment. To solve this numerical optimization problem the Non-dominated Sorting Genetic Algorithm II (NSGA-II) is chosen due to its robustness in providing optimal Pareto fronts (Deb et al., 2002). The NSGA-II algorithm provided in Seshadri (2020) is

[3] This is the sum of all 4 trips devised in the mission profile.

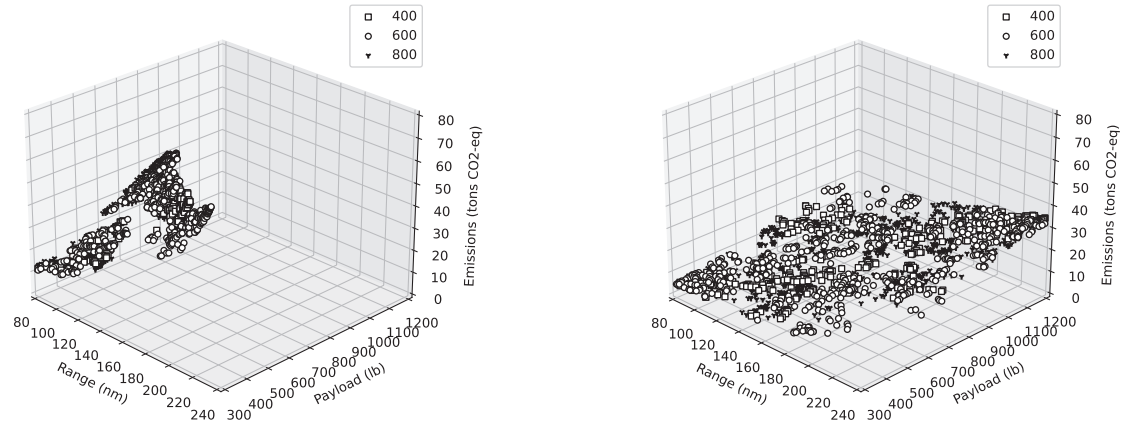

(a) All-electric (b) Hybrid-electric

Fig. 9. Effect of population size in the multi-objective optimization process (to note that the hybrid-electric version is for all-electric vertical flight with a all-combustion cruise using ATJ obtained from wheat grain).

used for this study.

4.1. Performance assessment

In order to better understand all effects, first only range and payload are considered as objectives, i.e. the resulting aircraft are evaluated without considering their carbon footprint. Moreover, no noise constraint is considered. This is due to the fact that it is important to assess first the potential of the selected aircraft configurations in the UAM segment from a performance perspective. This is especially important for the aircraft with all-electric propulsive systems, since the selected batteries have a much lower specific energy density than the biofuels and kerosene. For this reason, only the all-electric configurations are analyzed here.

The optimal range and payload results are tabulated in Table 7 and the full Pareto Front is illustrated in Fig. 8, where it is noted that all configurations yield feasible results for the established parameters. A population size of 400 and 300 generations are defined for running the NGSA-II algorithm, after evaluating the population size impact on the results (which is found to be low for a population above 200 individuals). For the delimited range and payload limits it is possible to mention that only the latter is fully meet with all configurations, while the former is only reached with a tilt-rotor configuration. These performance results are clearly constrained by the imposed constraints and boundary limits. For instance, all designs present wingspans very close to the 50 ft (15.24 m) limit, installed power values near the 670 hp (500 kW) limit, L/D and disk loading values also at their boundaries or very close to them. To note that the PAX value is the number of persons that the payload corresponds to (assuming 220 lb (100 kg) per PAX): if the aircraft is autonomous this value corresponds to the number of passengers. Additionally to the optimization results for the design mission, the number of 20 nm (37 km) trips possible to carry out with the available energy (including reserve) is estimated as well as the time of each 20 nm (37 km) trip.

In what concerns the range objective, the tilt-rotor configuration is able to cover a larger range distance (between 11% and 14%) for about the same weight (less than 2% difference) while carrying more payload (9%) than the remaining configurations and consuming less energy (between 2% and 7%). This is mainly due to the fact that a higher L/D is possible (between 12% and 25%), which allowed for a slightly faster and more efficient flight in cruise resulting in one more 20 nm (37 km) trip and less time to accomplish each 20 nm (37 km) trip.

As mentioned before all configurations are able to reach the maximum payload value (1200 lb (544 kg)) when this parameter has the highest importance in the multi-objective optimization, although the tilt-rotor design provides a higher range (between 13% and 16%) than the other configurations mainly due to the higher L/D (between 13% and 25%) as also noticed for the range objective.

Given the higher performance results obtained for the tilt-rotor as one can note from the Pareto Front (see Fig. 8), this configuration is chosen for the sustainability assessment.

4.2. Environmental sustainability

In this second study, the main goal is to evaluate the sustainability of UAM aircraft in terms of both pollutant and noise emissions, without neglecting the previously analyzed performance metrics and considering different energy sources: batteries; kerosene/jet fuel A; and biofuels. The population size is increased to account for the higher number of design variables utilized in the multi-objective optimization. From the Pareto Fronts obtained and illustrated in Fig. 9 one can notice that the results are not considerably changed, thus a medium population of 600 is used in the following calculations. For the hybrid-electric configuration, the electric version is for

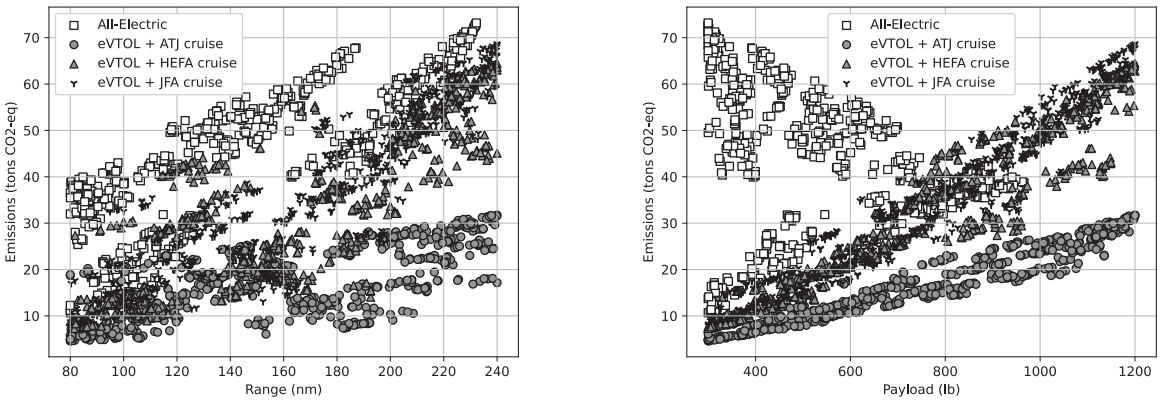

(a) Emissions vs. Range (b) Emissions vs. Payload

Fig. 10. Comparison of Pareto Fronts obtained using different energy sources.

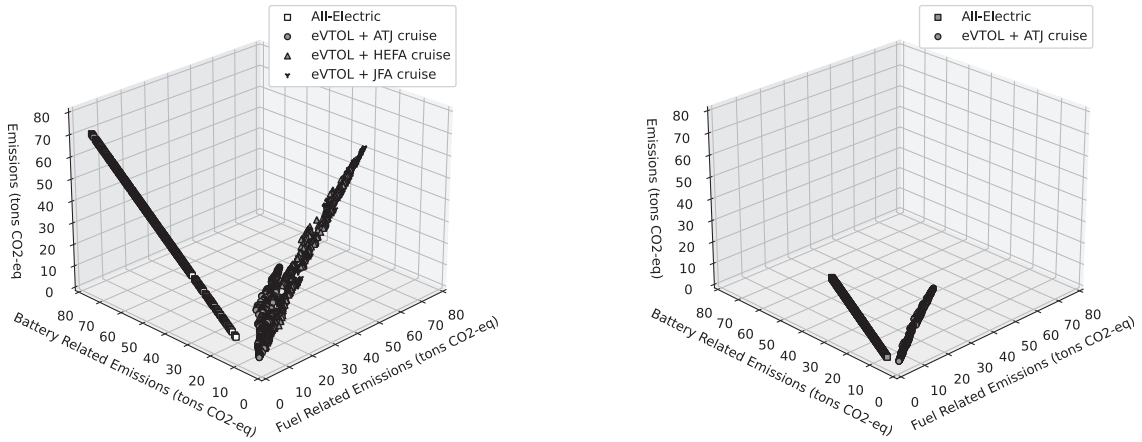

(a) EU-28 case (b) Swedish case

Fig. 11. Emissions breakdown.

all-electric vertical flight with an all-combustion cruise using ATJ obtained from wheat straw. This biofuel is considered due to the lower emissions comparing with the other biofuels and the similar energy density with conventional fuel.

From the Pareto Front obtained for the all-electric aircraft (Fig. 9 (a)) it is possible to observe three distinct areas. Each one corresponding to the maximization or minimization of one of the three established objectives: (1) the designs that minimize emissions have the lowest payload and range possible; (2) payload maximization is achieved when range takes the lowest value possible; (3) and range is maximized for the lowest payload value. These observations are less clear for the hybrid-electric aircraft (Fig. 9 (b)) since these designs are less constrained by the design variables' boundaries and constraints imposed, resulting in a broader design space which allowed to reach the maximum allowable range and payload. It is worth mentioning that the designs which maximize performance metrics are limited by the noise constraint and all designs are on (or very close to) their upper and lower limits of L/D and DL, respectively.

The first comparison, depicted in Fig. 10, is done considering an all-electric solution and 3 hybrid-electric solutions which for vertical flight run on batteries, while in cruise are powered by: ATJ obtained from wheat grain; HEFA obtained from jatropha; and Jet Fuel A (JFA).

When comparing the all-electric designs with the hybrid-electric ones powered by ATJ (obtained from wheat straw), one can clearly notice that by using this biofuel a higher performance (range and payload) can be delivered at the same time that less CO_2-eq is globally released into the atmosphere. The main reason for this outcome is related to the fact that ATJ obtained from wheat grain is one of the biofuels with the lowest impact to the environment (much lower than Jet Fuel A and the HEFA produced from jatropha as one can observe in Table 1). In fact, its production results in less 62% of CO_2-eq than the EU electric grid for the equivalent amount of energy. Although, this is not as clear in case of the aircraft running on Kerosene/Jet Fuel A and HEFA (obtained from jatropha). This issue

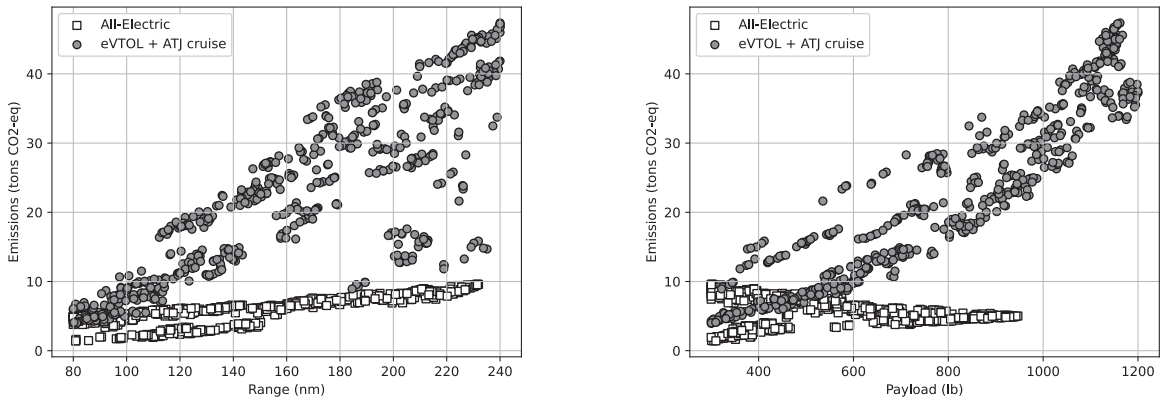

(a) Emissions vs. Range (b) Emissions vs. Payload

Fig. 12. Comparison of Pareto Fronts obtained using an all-electric solution and a hybrid-electric solution, considering a reduction on the emissions during the battery production phase and an improvement on the number of recharge–discharge cycles.

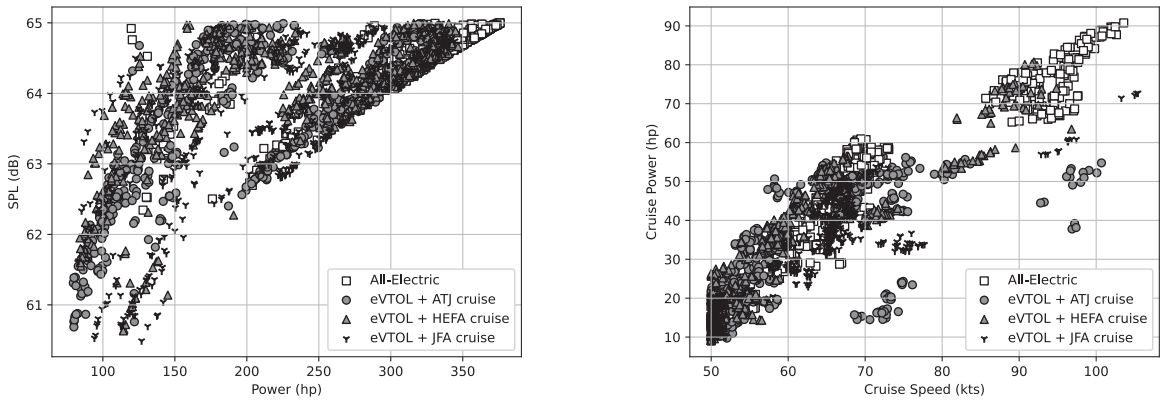

(a) SPL vs. Installed Power (b) Cruise Power vs. Cruise Speed

Fig. 13. Comparison of Pareto Fronts obtained using different energy sources.

becomes more noticeable when breaking down the emissions in battery and fuel related emissions as depicted in Fig. 11 (a). For the hybrid-electric aircraft, since batteries are only sized for vertical flight operation, this energy source does not contribute significantly to the total emissions. For these aircraft, fuel is the main contributor, especially due to its production that is estimated to emit substantially more CO_2-eq per the same about of energy than its consumption (by 3 orders of magnitude). The environmental impact of all-electric aircraft is profoundly dependable of energy source. For instance, when a higher percentage of renewable energy sources is employed to generate electricity such is the case of the Swedish electric grid (a value of 13 gCO_2/kW.h (European Environment Agency, 2020) is used here), this emission problem substantially reduces as one can notice in Fig. 11 (b).

Even though the emissions have considerably reduced to less than half of the EU-28 case, sustainable biofuels such as ATJ obtained from wheat straw still contribute less to the climate changes and global warming than an all-electric solution in the Swedish case. To further mitigate the impact of an all-electric UAM solution to the environment, not only the specific energy density should be improved, but also the number of cycles and the reduction of the impact of the production phase. Since major breakthroughs would be required to improve the specific energy density of the Li-S battery, optimistic values for the other two parameters were chosen, namely: the best case scenario of 17 $kgCO_2$-eq/kW.h for the emissions during the production phase from Arvidsson et al. (2018); and 1000 recharge–discharge cycles which according to Benveniste et al. (2018) are being tested in a European project. When employing these more optimistic values for the batteries and the Swedish electric grid, it is now possible to achieve lower contributions to the climate

changes and global warming using an all-electric solution as one can observe in Fig. 12. [4]

Both the maximum range and payload are reached with hybrid-electric propulsive systems running on different fuels, although these values are lower when all-electric propulsive systems are used, only 232 nm (430 km) and 966 lb (438 kg) (corresponding to 4 persons) are possible as maximum range and payload, respectively. These performance objectives are found to be limited by not only the SPL constraint (this is noticeable from Fig. 13 (a)), but also the upper and lower boundaries of the L/D and DL, respectively.

Power constraint is never active in the obtained Pareto Fronts (see Fig. 13 (a)) since the aircraft concepts are either limited by the noise constraint or the goal to minimize emissions which leads to a substantial installed power reduction (above 40%) in regard to the first study. Regardless of the selected propulsive system, the cruise speed takes similar values with more designs within 65 kts (33.4) (defined stall speed which is employed in one of the two possible requirements used to the size the wing area) and 100 kts (51.44 m/s), thus no major differences will be found on the time of each trip. Nevertheless, when the emission minimization objective is prioritized, the speed assumes values close to the lower limit (50 kts (25.7 m/s)). It is important to note that the cruise power is slightly lower than an average gasoline car.

5. Concluding remarks

A multidisciplinary low-fidelity computational framework has been developed to evaluate operational performance and environmental footprint of conceptual UAM designs. This framework can be integrated in an optimization environment to better explore the design space and to provide feasible and sustainable flight vehicle concepts for the UAM segment. Three different concepts were first optimized with respect to the performance goals (range and payload) for a given mission profile and considering an all-electric propulsion system. The tilt-rotor configuration is found to cover a larger range (between 11% and 14%) and consumes less energy (between 2% and 7%) compared to the tilt-wing and lift + cruise configurations, respectively. This was primarily attributed to the higher lift-to-drag ratio. Next, a hybrid-electric propulsive system was considered and the tilt-rotor configuration was optimized not only for range and payload maximization, but also for minimization of pollutant emissions and considering a noise limit of 65 dB. From a performance perspective, the all-electric propulsion system was found to be feasible for the UAM segment (it can carry up to 4 persons and covers 218 nm (404 km)), while being less competitive in terms of performance compared to an equivalent hybrid-electric version. Noise is found to limit the payload capacity of UAM aircraft concepts, especially for the all-electric versions due to the higher maximum take-off mass. Despite the focus was not on noise emissions directly, this was taken into account as a constraint. However, with different design considerations this may become a major limitation to the aircraft performance and sustainability. Biofuels show promise for this segment, especially the most sustainable ones such as ATJ obtained from wheat straw, as their emissions are lower compared to the conventional fossil fuels, and in cases where the electric grid does not rely mostly on renewable sources as is the case in the European Union. In order for all-electric aircraft to become competitive further improvements are required in the: (i) percentage of renewable energy sources in the electric grid; (ii) specific energy density of the batteries; (iii) number of recharge–discharge cycles; and (iv) raw materials used in the production of the batteries.

Acknowledgments

The authors acknowledge Fundação para a Ciência e a Tecnologia (FCT), through IDMEC, under LAETA, project UIDB/50022/2020. A.S. acknowledges the NSERC Canada Research Chair funding program.

References

Airbus S.A.S., 2020. Vahana, https://www.airbus.com/innovation/urban-air-mobility/vehicle-demonstrators/vahana.html (accessed: 2020-05-27).
Al Haddad, C., Chaniotakis, E., Straubinger, A., Plötner, K., Antoniou, C., 2020. Factors affecting the adoption and use of urban air mobility. Transp. Res. Part A: Policy Pract. 132, 696–712. https://doi.org/10.1016/j.tra.2019.12.020.
Arvidsson, R., Janssen, M., Svanström, M., Johansson, P., Sandén, B.A., 2018. Energy use and climate change improvements of li/s batteries based on life cycle assessment. J. Power Sources 383, 87–92. https://doi.org/10.1016/j.jpowsour.2018.02.054.
Aurora Flight Sciences, 2020. a Boeing Company, PAV – Passenger Air Vehicle, https://www.aurora.aero/pav-evtol-passenger-air-vehicle/ (accessed: 2020-05-27).
Bacchini, A., Cestino, E., 2019. Electric VTOL configurations comparison. Aerospace 6 (3), 26. https://doi.org/10.3390/aerospace6030026.
Benveniste, G., Rallo, H., Canals Casals, L., Merino, A., Amante, B., 2018. Comparison of the state of lithium-sulphur and lithium-ion batteries applied to electromobility. J. Environ. Manage. 226, 1–12. https://doi.org/10.1016/j.jenvman.2018.08.008.
Bini, M., Capsoni, D., Ferrari, S., Quartarone, E., Mustarelli, P., 2015. 1 – Rechargeable lithium batteries: key scientific and technological challenges. In: Franco, A.A. (Ed.), Rechargeable Lithium Batteries, Woodhead Publishing Series in Energy, Woodhead Publishing, pp. 1–17. doi:10.1016/B978-1-78242-090-3.00001-8.
Boeing Company, 2020. V-22 Osprey, http://www.boeing.com/defense/v-22-osprey/ (accessed: 2020-05-27).
Brown, A., Harris, W., 2018. A vehicle design and optimization model for on-demand aviation. In: AIAA/ASCE/AHS/ASC Structures, Structural Dynamics, and Materials Conference, Kissimmee, FL, USA. doi:10.2514/6.2018-0105.
Chuck, C.J., 2016. Biofuels for Aviation: Feedstocks, Technology and Implementation, Academic Press, London, UK. doi:10.1016/C2014-0-03505-8.
Cork, T.C., 2003. Design of Aircraft. Prentice Hall, New Jersey, USA.
Deb, K., Pratap, A., Agarwal, S., Meyarivan, T., 2002. A fast and elitist multiobjective genetic algorithm: NSGA-II. IEEE Trans. Evol. Comput. 6 (2), 182–197. https://doi.org/10.1109/4235.996017.
de Jong, S., Antonissen, K., Hoefnagels, R., Lonza, L., Wang, M., Faaij, A., Junginger, M., 2017. Life-cycle analysis of greenhouse gas emissions from renewable jet fuel production. Biotechnol. Biofuels 10, 64. https://doi.org/10.1186/s13068-017-0739-7.
Deming, A.F., 1940. Propeller rotation noise due to torque and thrust, Tech. Rep. TN 747, NACA.

[4] It is worth to note that since the number of recharge–discharge cycles have increased the number of missions have also increased, leading to a higher overall emissions.

Eißfeldt, H., 2020. Sustainable urban air mobility supported with participatory noise sensing. Sustainability 12, 3320. https://doi.org/10.3390/su12083320.
EPA, 2020. United States Environmental Protection Agency, Greenhouse Gases Equivalencies Calculator – Calculations and References, https://www.epa.gov/energy/greenhouse-gases-equivalencies-calculator-calculations-and-references [accessed: 2020-06-25].
European Comission, 2020. Horizon 2020 – Work Programme 2018–2020, 11. Smart, Green and Integrated Transport, https://ec.europa.eu/research/participants/data/ref/h2020/wp/2018-2020/main/h2020-wp1820-transport_en.pdf, accessed: 2020-06-03.
European Environment Agency, 2020. Overview of electricity production and use in europe, https://www.eea.europa.eu/data-and-maps/indicators/overview-of-the-electricity-production-2/assessment-4 (accessed: 2020-07-02).
Finger, D.F., Braun, C., Bil, C., 2019. Impact of electric propulsion technology and mission requirements on the performance of vtol uavs. CEAS Aeronaut. J. 10, 827–843. https://doi.org/10.1007/s13272-018-0352-x.
Fu, M., Rothfeld, R., Antoniou, C., 2019. Exploring preferences for transportation modes in an urban air mobility environment: Munich case study. Transp. Res. Rec. 2673 (10), 427–442. https://doi.org/10.1177/0361198119843858.
Gawron, T.B.B., 2018. Impact of a Jet A-1/HEFA blend on the performance and emission characteristics of a miniature turbojet engine. Int. J. Environ. Sci. Technol. 15, 1501–1508. https://doi.org/10.1007/s13762-017-1528-3.
GEVO, 2019. Sustainable aviation fuel: Alcohol-to-jet synthetic paraffinic kerosene is a proven pathway to deliver a bio-based, low-carbon option to travelers, https://gevo.com/wp-content/uploads/2020/05/Gevo-Whitepaper-Sustainable-Aviation-Fuel.pdf (accessed: 2020-06-28).
Gutiérrez-Antonio, C., Gómez-Castro, F.I., de Lira-Flores, J.A., Hernández, S., 2017. A review on the production processes of renewable jet fuel. Renew. Sustain. Energy Rev. 79, 709–729. https://doi.org/10.1016/j.rser.2017.05.108.
Gutin, L., 1948. On the sound field of a rotating propeller, Tech. Rep. TM 1195, NACA.
Han, J., Elgowainy, A., Cai, H., Wang, M.Q., 2013. Life-cycle analysis of bio-based aviation fuels. Bioresour. Technol. 150, 447–456. https://doi.org/10.1016/j.biortech.2013.07.153.
Hepperle, M., 2012. Electric flight-potential and limitations. In: Energy Efficient Technologies and Concepts of Operation, Lisbon, Portugal.
International Energy Agency (IEA), 2019. CO2 Emissions from Fuel Combustion 2019 Highlights, https://webstore.iea.org/co2-emissions-from-fuel-combustion-2019-highlights (accessed: 2020-06-25).
International Air Transport Association, 2015. IATA 2015 Report on Alternative Fuels, https://www.iata.org/contentassets/462587e388e749eeb040df4dfdf02cb1/2015-report-alternative-fuels.pdf, ISBN 978-92-9252-870-6, Montreal-Geneva.
Johnson, W., 2010. NDARC – NASA design and analysis of rotorcraft validation and demonstration. In: American Helicopter Society Aeromechanics Specialists' Conference, San Francisco, CA, USA.
Johnson, W., 2013. Rotorcraft Aeromechanics. Cambridge University Press, New Year, NY, USA.
Johnson, W., Silva, C., Solis, E., 2018. Concept vehicles for vtol air taxi operations. In: AHS Technical Conference on Aeromechanics Design for Transformative Vertical Flight, San Francisco, CA, USA.
Jungbluth, N., Meili, C., 2019. Recommendations for calculation of the global warming potential of aviation including the radiative forcing index. Int. J. Life Cycle Assess. 24, 404–411. https://doi.org/10.1007/s11367-018-1556-3.
Kousoulidou, M., Lonza, L., 2016. Biofuels in aviation: fuel demand and co2 emissions evolution in europe toward 2030. Transp. Res. Part D: Transp. Environ. 46, 166–181. https://doi.org/10.1016/j.trd.2016.03.018.
Kuhn, H., Seitz, A., Lorenz, L., Isikveren, A.T., Sizmann, A., 2012. Progress and perspectives of electric air transport. In: 28th International Congress of the International Council of the Aeronautical Sciences ICAS, Brisbane, Australia.
Lokesh, K., Sethi, V., Nikolaidis, T., Goodger, E., Nalianda, D., 2015. Life cycle greenhouse gas analysis of biojet fuels with a technical investigation into their impact on jet engine performance. Biomass Bioenergy 77, 26–44. https://doi.org/10.1016/j.biombioe.2015.03.005.
Lukaczyk, T.W., Wendorff, A.D., Colonno, M., Economon, T.D., Alonso, J.J., Orra, T.H., Ilario, C., 2015. SUAVE: an open-source environment for multi-fidelity conceptual vehicle design. In: 16th AIAA/ISSMO Multidisciplinary Analysis and Optimization Conference, Dallas, TX, USA. doi:10.2514/6.2015-3087.
Marte, J.E., Kurtz, D.W., 1970. A review of aerodynamic noise from propellers, rotors, and lift fans, Tech. Rep. 32–1462, Jet Propulsion Laboratory, California Institute of Technology, Pasadena, California, USA.
McDonald, R., German, B., 2017. German, eVTOL Stored Energy Overview. In: Uber Elevate Summit, Dallas, Texas, USA.
Mueller, E.R., Kopardekar, P.H., Goodrich, K.H., 2017. Enabling airspace integration for high-density on-demand mobility operations. In: 17th AIAA Aviation Technology, Integration, and Operations Conference, Denver, Colorado, USA. https://doi.org/10.2514/6.2017-3086.
Neuling, U., Kaltschmitt, M., 2018. Techno-economic and environmental analysis of aviation biofuels. Fuel Process. Technol. 171, 54–69. https://doi.org/10.1016/j.fuproc.2017.09.022.
Ng, W., 2019. An Experimental and Analytical Investigation of Hydrogen Fuel Cells for Electric Vertical Take-Off and Landing (eVTOL) Aircraft. Master thesis. University of Maryland.
Patterson, M.D., German, B.J., Moore, M.D., 2012. Performance analysis znd design of on-demand electric aircraft concepts. In: 12th AIAA Aviation Technology, Integration, and Operations (ATIO) Conference and 14th AIAA/ISSMO Multidisciplinary Analysis and Optimization Conference, Indianapolis, IN, USA. https://doi.org/10.2514/6.2012-5474.
Pornet, C., Gologan, C., Vratny, P.C., Seitz, A., Schmitz, O., Isikveren, A.T., Hornung, M., 2015. Methodology for sizing and performance assessment of hybrid energy aircraft. J. Aircraft 52 (1), 341–352. https://doi.org/10.2514/1.C032716.
Prussi, M., O'Connell, A., Lonza, L., 2019. Analysis of current aviation biofuel technical production potential in EU28. Biomass Bioenergy 130, 105371. https://doi.org/10.1016/j.biombioe.2019.105371.
Raymer, D.P., 1992. Aircraft Design: A Conceptual Approach. American Institute of Aeronautics and Astronautics Inc, Washington, DC, USA.
Ribeiro, J., Afonso, F., Ribeiro, I., Ferreira, B., Policarpo, H., Peças, P., Lau, F., 2020. Environmental assessment of hybrid-electric propulsion in conceptual aircraft design. J. Cleaner Prod. 247, 119477. https://doi.org/10.1016/j.jclepro.2019.119477.
Rothfeld, R., Straubinger, A., Fu, M., Al Haddad, C., Antoniou, C., 2020. Chapter 13 – urban air mobility. In: Antoniou, C., Efthymiou, D., Chaniotakis, E. (Eds.), Demand for Emerging Transportation Systems. Elsevier, pp. 267–284. https://doi.org/10.1016/B978-0-12-815018-4.00013-9.
Schäfer, A.W., Barrett, S.R.H., Doyme, K., Dray, L.M., Gnadt, A.R., Self, R., O'Sullivan, A., Synodinos, A.P., Torija, A.J., 2019. Technological, economic and environmental prospects of all-electric aircraft. Nature Energy 4, 160–166. https://doi.org/10.1038/s41560-018-0294-x.
Schlegel, R., King, R., Muli, H., 1966. Helicopter rotor noise generation and propagation, Tech. Rep. 66–4, US Army Aviation Material Laboratories, Fort Eustis, VA, USA.
Seshadri, A., 2020. NSGA – II: A multi-objective optimization algorithm, https://www.mathworks.com/matlabcentral/fileexchange/10429-nsga-ii-a-multi-objective-optimization-algorithm (accessed: 2020-06-09).
Staples, M.D., Malina, R., Suresh, P., Hileman, J.I., Barrett, S.R., 2018. Aviation co2 emissions reductions from the use of alternative jet fuels. Energy Policy 114, 342–354. https://doi.org/10.1016/j.enpol.2017.12.007.
STM International, 2020. ASTM D7566–20, Standard Specification for Aviation Turbine Fuel Containing Synthesized Hydrocarbons, https://www.astm.org/Standards/D7566.htm (accessed: 2020-06-26).
Thipphavong, D.P., Apaza, R., Barmore, B., Battiste, V., Burian, B., Dao, Q., Feary, M., Go, S., Goodrich, K.H., Homola, J., Idris, H.R., Kopardekar, P.H., Lachter, J.B., Neogi, N.A., Ng, H.K., Oseguera-Lohr, R.M., Patterson, M.D., Verma, S.A., 2018. Urban air mobility airspace integration concepts and considerations. In: 2018 Aviation Technology, Integration, and Operations Conference, Atlanta, Georgia, USA. https://doi.org/10.2514/6.2018-3676.
Torija, A.J., Li, Z., Self, R.H., 2020. Effects of a hovering unmanned aerial vehicle on urban soundscapes perception. Transp. Res. Part D: Transp. Environ. 78, 102195. https://doi.org/10.1016/j.trd.2019.11.024.
Vascik, P.D., Hansman, R.J., Dunn, N.S., 2018. Analysis of urban air mobility operational constraints. J. Air Transp. 26 (4), 133–146. https://doi.org/10.2514/1.D0120.

Vegh, J.M., Botero, E., Clark, M., Smart, J., Alonso, J.J., 2019. Current capabilities and challenges of ndarc and suave for evtol aircraft design and analysis. In: AIAA Propulsion and Energy Forum, Indianapolis, IN, USA. https://doi.org/10.2514/6.2019-4505.
Vertical Flight Society, 2020. eVTOL Classifications, https://evtol.news/classifications/ (accessed: 2020-03-11).
Vertical Flight Society, 2020. Joby S2 (defunct), https://evtol.news/aircraft/joby-s2/ (accessed: 2020-05-27).
Wisk Aero LLC, 2020. Cora by Wisk, https://wisk.aero/cora/ (accessed: 2020-05-27).
Wolff, D., Casals, L.C., Benveniste, G., Corchero, C., Trilla, L., 2019. The effects of lithium sulfur battery ageing on second-life possibilities and environmental life cycle assessment studies. Energies 12 (12), 2440. https://doi.org/10.3390/en12122440.
Zhou, Y., Zhao, H., Liu, Y., 2020. An evaluative review of the vtol technologies for unmanned and manned aerial vehicles. Comput. Commun. 149, 356–369. https://doi.org/10.1016/j.comcom.2019.10.016.
Zubi, G., Dufo-López, R., Carvalho, M., Pasaoglu, G., 2018. The lithium-ion battery: state of the art and future perspectives. Renew. Sustain. Energy Rev. 89, 292–308. https://doi.org/10.1016/j.rser.2018.03.002.